Identification of potent VEGFR-2 Inhibitors of Angiogenesis through homology modeling, structure based virtual screening, docking and molecular dynamics simulations

Madhu Sudhana Saddala, J. Obaiah, A. Usha Rani

Abstract— VEGFR-2 is a known protein target for antiangiogenic agents, was used in this study. In order to understand of the mechanisms of ligand binding and the interaction between the ligand and the VEGFR-2. A three-dimensional (3D) model of the VEGFR-2 is generated based on the crystal structure of the complex containing KIT and sunitinib (PDB code 3G0E) by using the Moduller9v11 software. With the aid of the MD simulation methods, the final refined model is obtained and is further assessed by SAVES server, which shows that the refined model is reliable. With this model, a flexible docking with screened compounds from Zinc database was performed by AutoDock in PyRx Virtual Screening tool. Ten lead molecules having better binding energy than query (Pazopanib). The binding interactions of compounds with active site of VP-3 model suggested that the amino acid residues (Glu13, Glu15, Leu57, Glu134, Cys136, Lys137, Gly215, Arg218, Asp 223, Arg247 and Tyr249) play a key role for drug design. The MD simulations were performed for VEGFR-2-Zinc14945139 (lead1) docking complex in NAMD v2.9. The Trajectory analysis showed docking complex and inter molecular interactions was stable throughout the entire production part of MD simulations. The predicted pharmalogical properties of best compounds, among them Zinc14945139 is well within the range of a drug molecule with good ADME profile. Hence, would be intriguing towards development of potent inhibitor molecule against VEGFR-2.

Index Terms— VEGFR-2, MD simulations, Molecular docking, Homology modeling, Zinc database, NAMD, VMD.

———————————— ◆ ————————————

1 INTRODUCTION

Cadmium (Cd) is classified as a Type I human carcinogen and its causes angiogenesis. It is the process of growing new blood vessels from the preexisting ones [1]. It is not only important for normal physiological functioning but also critical for many pathological processes such as tumor initiation, proliferation, and metastasis [2, 3, 4]. It has been well established that angiogenesis is a fundamental requirement for tumor development. Studies have demonstrated that vascular endothelium could be a primary target of Cd toxicity [1, 4]. Some studies reported disruptive effects of Cd on human endothelial cells [5, 6]. The effect of Cd on reactive oxygen species (ROS), mitogen-activated protein kinases/extracellular signal-regulated kinases (MAPK/ERK), AKT, and p70S6K1 signaling pathways and the downstream proangiogenic factors hypoxia-inducible factor-1 (HIF-1) and VEGF in human lung epithelial cells. VEGF exerts its biological actions by binding to its two receptor tyrosine kinases expressed on endothelial cells, namely, VEGFR-1 (Flt-1) and VEGFR-2 (KDR/Flk-1). VEGFR-1 is poorly autophosphorylated in response to VEGF in endothelial cells and is weakly involved in transducing the VEGF angiogenic signals. The evidences support the concept that VEGFR-1 might act as a decoy receptor rather than as a signal transducing molecule [7, 8], whereas ligand-induced homodimerization of VEGFR-2 leads to a strong autophosphorylation of several [9] tyrosine residues of VEGFR-2. It is essential for the morphogenesis of vascular endothelium and is the primary receptor mediating the angiogenic activity of VEGF through distinct signal transduction pathways that regulate endothelial cell proliferation, migration, differentiation and tube formation [10, 11]. The VEGFR-2 signaling pathway is a promising target of angiogenesis, because it is a common pathway for tumor-induced angiogenesis [12]. VEGF is viewed as an attractive therapeutic target for the development of novel anticancer agents [41]. There are several angiogenesis inhibitors in phase I or phase II clinical trials, including antibodies aimed at VEGF or VEGFRs [13, 14], soluble decoy receptors that sequester ligands [40] and small molecule inhibitors that inhibit [15] kinase activity. To exploit more efficient and safer agents for the treatment of angiogenesis-related diseases such as cancer, a large number of scholars have been actively pursuing small molecule therapeutic strategies targeted at VEGFR-2-mediated [16, 17] signal transduction pathway. In this study we use Pazopanib natural drug as a query screening compounds from drug databases. Pazopanib, which is being developed by GlaxoSmithKline plc, is an oral, second-generation multi-targeted tyrosine kinase inhibitor that targets VEGFR, platelet-derived growth factor receptor and c-kit, key proteins responsible for tumor growth and survival. Pazopanib exhibited good potency against all of the human VEGFRs and closely related tyrosine receptor kinases in vitro, and demonstrated antitumor activity in several human tumor xenografts, including renal cell carcinoma (RCC), and breast and lung cancer. In phase I and II clinical trials, Pazopanib was generally well tolerated with the main side effects being hypertension, fatigue or gastrointestinal disorders. Pazopanib alone caused a decrease in tumor size and stable disease in a significant number of patients, including those with RCC, NSCLC and gynecological tumors [18]. Finally, a virtual screening experiment was carried out to validate the effectiveness of the model and its ability to retrieve actives

seeded in a compound collection of 35000 decoys.

Therefore, an attempt was made to develop the novel and potent inhibitors against VEGFR-2 in angiogenesis through computational approaches such as homology modeling, molecular docking, molecular dynamics (MD) simulations, QSAR and structure based virtual screening studies.

2 MATERIALS AND METHODS

2.1 Physicochemical properties

Protein sequence of VEGFR-2 (Accession: P35968.2) of human was retrieved in the FASTA format from NCBI database. Physicochemical properties such as aliphatic index, Grand average of hydropathy (GRAVY), Theoretical pI value of VEGFR-2 were calculated using PROTPARAM.
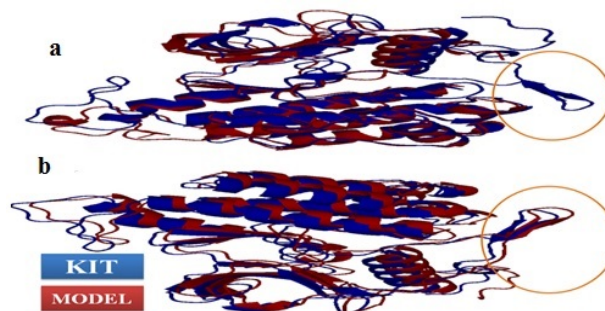
2.2 VEGFR-2 model

The X-ray structures of VEGFR-2 in the PDB (3EWH) do not contain the loop after the DFG motif, which includes residues from 1048 to 1068 [19]. The X-ray structure denoted by 3EWH in the PDB contains some residues of this loop; their positions are similar to the positions of the analogue residues in the tyrosine-protein kinase KIT (PDB: 3G0E) (Fig.1). Keeping in view, a new VEGFR-2 model consists of this loop was built using homology modeling by using MODELLER 9v11 [20] on the basis of co-ordinates of KIT (PDBID: 3G0E) as a template. The resulting loop structure is shown in Figure1B. Computations were run on a quad core Intel 3.0 GHz Xeon X5472 processor.

Fig. 1: Comparison between VEGFR-2 and KIT. (a) Superimposition of the analogous loops of VEGFR-2 and KIT (PDB: 3G0E). (b) Superimposition of the analogous loops of VEGFR-2 and KIT after homology modeling (VEGFR-2 in red and KIT in blue).

2.3 Homology modeling

The crystal structure of KIT (PDB: 3GOE) was selected [19] as a template to model the VEGFR-2. Sequence alignment between 3EWH and 3GOE sequences was performed using [21]. ClustalW and was further optimized manually (Fig.2). This alignment was employed for model construction with the comparative [20, 22] modeling software MODELER9v11. All models were built with a medium-level loop refinement, and the discrete optimized protein energy (DOPE) potentials [23] were calculated for subsequent evaluation. The last modeller objective (low dope score) obtained was analyzed through Ramachandran plot to check the stereo chemical quality of protein structure using PROCHECK [24], environment profile using verify_3D [25] and ERRAT [26].The residue packing and

_____

- *Prof. A. Usha Rani, Dept. of Zoology, Sri Venkateswra University, Tirupati-517502. E-mail: aur_svu9@yahoo.co.in*

- *Madhu Sudhana Saddala is currently pursuing Doctor of Phylosophy program in Bioinformatics, Sri Venkateswara University, India, PH-09542412717. E-mail: madhubioinformatics@gmail.com*

atomic contacts were analyzed using WHATIF [27] and Z

score of Ramachandran plot was analyzed using WHATCHECK [28]. The resulting VEGFR-2 model was further refined by the energy minimization and MD simulations.

2.4 Refinement of homology model

The initial model was refined with MD simulation which was carried out with the Visual Molecular Dynamics (VMD) tool [29]. The CHARMM 27 field [30] was used for parameterization and the program NAMD [31] was used for all energy minimization and molecular dynamics (MD) simulations. All of the MD simulations were carried out in explicit water, employing periodic boundary conditions. The system was first energy minimized for 1000 steps with atoms of VEGFR-2 fixed, and then energy minimization was performed for 2500 steps.

2.5 Simulation parameters

The MD simulations system was equilibrated at 250 k for 10 ps with VEGFR2 atoms fixed, followed by 20 ps MD without restraints. The system was subsequently simulated for 100 ps at 300 k with the following parameters. The classical equations of motion were integrated by a leap frog integrator using a time step at 1fs. The impulse based ver let-I/r-RESPA method was used perform multiple time stepping: 4 fs long-range electrostatic: 2fs for short range non-bonded forces, and 1 fs for bonded force [31]. The swift function was used to cutoff the Lennard-Jones potential, with the first cut off at 10 Å and the second cutoff at 12 Å. Short range interactions were calculated at intervals of 4 fs. All bonds involving hydrogen atoms were constrained to their equilibrium bond parameters using the SHAKE along them. Langevin dynamics were employed to maintain the pressure at 1 atm, with a Langevin pisten period of 100 fs and oscillation decay time of 50 fs. Trajectories were recorded every 200 fs. Subsequently the dynamics behavior and structural changes of the protein was analyzed by the calculation of energy and the root mean square deviation (RMSD).

2.6 Assessment of the homology model

Models were generated using the ClustalW alignment of the template and the sequence depicted in Fig.2, followed by refinement with energy minimization and limited constrained MD simulations with an implicit solvent model. To assess the models before and after the simulations, we employed DOPE score, ERRAT (Fig.4), Verify_3D (Fig.5) scores and

PROCHECK (Table1). DOPE is an atom-based statistical potential, representing the conformational energy that measures the relative stability of a conformation with respect to other conformations of the same protein. Verify_3D scores were used to assess whether a residue is in the desired 3D environment. The "environment" is based on buried area, secondary structure, and fraction of polar contacts. Furthermore, having included the "Add Membrane" routine, the low-dielectric environment of the bilayer was taken into consideration in the Verify_3D calculations; amino acids embedded in the implicit membrane boundary were considered fully buried. A low score is given to a hydrophobic residue on a protein's surface and a polar residue in the protein's core. A model region with a score higher than the expected values are likely to be correct, but a score lower than the expected values should be carefully examined. Comparison of all constructed models led us to select the one with the lowest DOPE and highest Verify_3D scores (data not shown). It should also be mentioned that a substantial improvement of both DOPE and Verify scores was observed for this model following refinement (Verify_3D scores rose from 65.43 to 90.66, as shown in Table1). It was pleasing to see that the resultant model was within the expected range of the Profiles-3D scoring function, thus suggesting that the residues are placed in a physically acceptable environment after refinement. PROCHECK was also used in order to check the stereochemical quality of the model-built structures. Ramachandran plots were generated within PROCHECK to highlight regions with unusual geometry and provide an overall assessment of the quality of the model. It can be seen that almost all residues in the model structures are in favored regions, and only 0.4% falls in the disallowed regions (Fig.3). Also RMSD values between superimposed model and crystallographic structure were calculated by using superpose program. VMD was used to analyze the molecular dynamics trajectory. The protein atoms in all of the frames were superimposed on the first frame of the trajectory to remove global rotational and translational movements. The root mean square deviation (RMSD) was calculated with reference to the starting structure. The PyMol molecular viewer (http://www.pymol.org/) was employed to analyze the docked structures.

Fig. 2: Sequence alignment of 3G0E with VEGFR-2 (PDB code 3EWH). Identical residues, similar residues and conservative residues highlight different colours.

Fig.3: A Ramachandran plot calculation of VEGFR-2 was performed using PROCHECK server.
Fig. 4: 3D profiles of VEGFR-2 were verified using ERRAT server. Overall quality score indicates residues are reasonably folded.
Fig.5: 3D profiles of VEGFR-2 verified with Verify_3D server.
Fig.6: Residues comprising the active sites of VEGFR2 and KIT in complex
Fig.7: Both Zinc and PubChem lead compounds superimposed in active site of VEGFR-2
Fig.8: VEGFR-2 domains represented in different colours, red indicates Phosphorylase Kinase domain and green indicates Phosphotransferase domain.
Fig.9: RMSD of protein backbone atom and ligand with respect to time over the course of the 10 ns MD simulations run (VEGFR-2- Zinc14945139 (lead1) complex).

2.7 Active site Identification

Active site of VEGFR-2 was identified using CASTp server (Computer Atlas of Surface Topology of protein) [32]. A new program, CASTp, for automatically locating and measuring protein pockets and cavities, is based on precise computational geometry methods, including alpha shape and discrete flow theory. CASTp identification and measurements of surface accessible pockets as well as interior inaccessible cavities by locating, delineating and measuring concave surface regions on three-dimensional structure of proteins (Fig.6). The measurement includes the area and volume of pocket or void by solvent accessible surface model (Richards' surface) and by molecular surface model (Connolly's surface), calculated analytically. It can also be used to study surface features and functional regions of protein.

2.8 Screening Ligands

Commercially available ligands are listed in public databases, such as ZINC database [39] that contains more than 4.6 million compounds in ready to dock and provide 3D formats at the URL http://ZINC.dock.org/. Virtual screening has been emerged as a complementary approach to high throughput screening and has become an important in silico technique in the pharmaceutical industry [33]. The structure based virtual screening begins with the identification of potential ligand binding sites on the target proteins. Usually, molecules that meet the criteria for biological activity fulfill characteristics contained in the Lipinski's rule of five [34], or the more relaxed rules revised by Veber et al., 2002 [35].

In our work, we have selected 35000 from Zinc database based on structure similarity of query Pazopanib natural compound. The AutoDock in PyRx Virtual Screening Tool URL http://pyrx.scripps.edu/ [36, 37] was used for the energy minimization of screened ligands.

2.9 Ligands-Protein docking studies

Docking is a computational method which predicts the preferred orientation of one molecule to a second when bound to

3EWH_/1-314
3G0E_/1-336

Fig.3 Ramachandran Plot VEGFR2
Fig.5
Fig.4
Fig.6
Fig.8
Fig.9
Fig.7
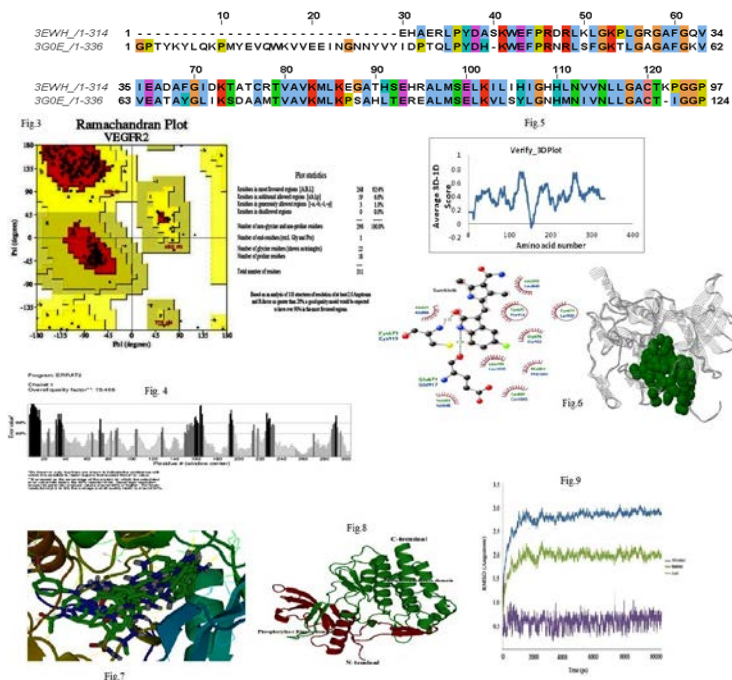
each other to form a stable complex. Docking has been widely used to suggest the binding modes of protein inhibiters. Most docking algorithms are able to generate a large number of possible structures, thus they also require a means to score each structure to identify those that of greatest interest. Docking was performed using AutoDock in PyRx Virtual Screening tool [36, 37].

Zinc screened compounds were docked into active site of refined model. Lamarkian genetic algorithm was used as number of individual population (150), max number of energy evaluation (25000000), max number of generation (27000) [24], Gene mutation rate (0.02), crossover rate (0.8), Cauchy beta (1.0) and GA window size (10.0).The grid was set whole protein due to the multi binding pocket at X=3.42, Y=-56.23, Z=98.32 and dimension Å) at X=89.92, Y=98.56, Z=98.32 and exhaustiveness 8. The pose for a given ligands identified on the basis of highest binding energy. Only ligand flexibility was taken into account and the proteins were considered to be rigid bodies. The resulting complexes were clustered according to their root mean square deviation (RMSD) values and binding energies, which were calculated using the AutoDock scoring function. Further characterization via molecular dynamics (MD) simulations was conducted using complexes that were selected according to their binding energy values and the interactions made with the surrounding residues. The PyMol molecular viewer (http://www.pymol.org/) was employed to analyze the docked structures.

2.10   MD simulation of of the VEGFR-2 - ligand complex

The VEGFR-2-ligand complex was placed in TIP3P water box, with distance of at least 15Å imposed between the solute atoms and the edge of the box. The position of the solute atoms were fixed during the first energy minimization for 1000 steps and no atoms were fixed during the second energy minimization for 1000 steps. MD simulation of the complex was carried out with the aforementioned protocol. The equilibrated system was subjected to 10 ns MD at 300K.

3   RESULTS AND DISCUSSION

3.1 Physicochemical Properties of VEGFR-2

Protein sequence of VEGFR-2 (Accession: P35968.2) of human was retrieved in FASTA from NCBI database. Physicochemical properties of VEGFR-2 contain 334 residues with the molecular weight of 2542.01, Aliphatic index, Grand average of hydropathy (GRAVY) and Theoretical pI value of the protein were found to be 43.63, 0.311 and 9.21 respectively.

3.2 Secondary structure prediction of VEGFR-2

The secondary structure elements of model VEGFR-2 consist of total 334 amino acids and the results of predicted structure with three different servers were shown in Table2. The secondary structure analysis has shown 25.38% alpha helix with 84 residues by GOR4, 41.99% with 139 residues by SOPMA, 42.90% with 142 residues by SOPM. Extended beta strands exhibit 12.99% with 43 residues by using SOPMA, 12.99% with 43 residues using SOPM and 21.75% with 72 residues using

GO4. The predicted values for beta turn were found to be 8.46% with 28 residues using SOPMA, 10.88% with 36 residues using SOPM and GOR4 fails to provide any prediction for beta turn. Random coils strands exhibit 36.56% with 121 residues by using SOPMA, 33.23% with 110 residues using SOPM and 52.87% with 175 residues using GO4 (Table1).

3.3 3D model contruction and validation

In this sense, a new model containing this loop was built using homology modeling by program MODELLER 9v11 (Sali and Blundell, 1993) and the structure of KIT as a template. Coordinates of structurally conserved regions (SCRs), structurally variable regions (SVRs), N-termini and C-termini from the template were assigned to the target sequences based on the satisfaction of spatial restraints. All side chains of the model protein were set by rotamers. Hundred models were generated using MODELLER9v11. Least DOPE score structure was chosen for structural evaluation.

The secondary structure prediction of VEGFR-2 by above mentioned servers. We identified secondary structural elements such as 2-sheets, 4-beta hairpins, 3-beta bulges, 7-strands, 15-helices, 22-beta turns, 3-gamma turns. Stereo chemical quality of the model was elucidated by PROCHEK sever. Ramachandran plot showed that 92.4% residues were plotted within the most favored region, 6.6% of residues were located within the additionally allowed region, 1.0% of residues within generally allowed region and 0.0% of residues within disallowed region (Fig.3). By adapting Whatcheck program the calculated values of Z-score for bond lengths-0.941, bond distances-0.019, bond angle-1.203, Omega angle restraints-0.735, Improper dihedral distribution-0.856, Inside/Outside distribution-1.059, dihedral RMS Z-score-0.856 were found respectively. Thus, these z-score values are positive than average. The overall quality factor of 75.466% was observed by using of ERRAT (Fig.4) environmental profile. Varify_3D (Fig.5) showed that 90.66% of all residues had an average 3D-1D score greater than 2 indicating that model was highly reliable. The constructed 3D model was superimposed with template using SPDBV software (Fig.1). RMSD of the model structure was 0.25 Å which indicates the reliability of the good model. Fig.6 showed active site of VEGFR-2, residues such as Glu13, Glu15, Leu57, Glu134, Cys136, Lys137, Gly215, Arg218, Asp 223, Arg247 and Tyr249 respectively.

Table1: ERRAT, Verify_3D, and PROCHECK Scores, before and after Minimization of VEGFR-2 (DOPE score = -38712. 25)

S.No.	Validation Servers	Minimization		Results
		before	after	
1	ERRAT	60.34	75.466	pass
2	Verify_3D	65.43	90.66	Pass
3	PROCHECK	85.7	92.4	Pass

3.4 Sructure of VEGFR-2

VEGFR-2 is a type III receptor tyrosine kinase of the

PDGFR family [PDGFRα/β, c-Kit, FLT3, and CSF-1 (cFMS)]. The majority of VEGFR-2 intracellular domains contain tyrosine residues (Tyr or Y) that are involved in redundant actions on vasculogenesis or angiogenesis [10]. The VEGFR-2 model was also divided into two parts viz. Phosphorylase Kinase domain and Transferase (Phosphotransferase) domain. The Phosphorylase Kinase domain (815-918residues; in our model indicates 1-103 residues) consists of 4 alpha helices and 5 beta sheets. This domain may involve in regulation of endothelial cell proliferation. The Transferase (Phosphotransferase) domain (919-1166; in our model indicates 104-331). It contains 10 alpha helices and 2 beta sheets. This domain may also involve in regulation of endothelial cell migration. These two domains are playing a key role in angiogenesis mechanism. In our study both domains were structurally, functionally illustrated and developed novel inhibitors. Fig.8 represented the N, C terminals and two domains.

Table2: Secondary structure Elements of VEGRF-2 was predicted by using different servers.

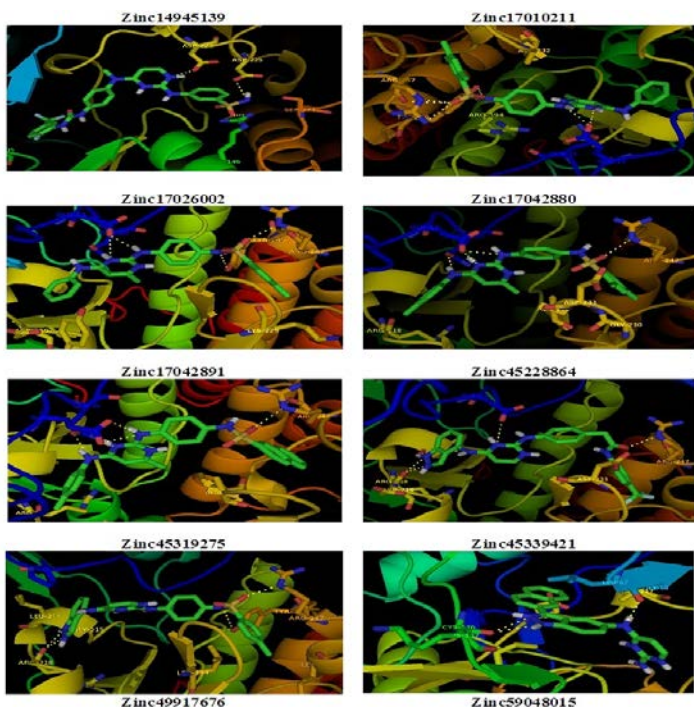| Secondary structure elements	SOPMA		GOR4		SOPM	
	Percentage%	Amino acids	Percentage %	Amino acids	Percentage %	Amino acids
Alpha helix	41.99%	139	25.38%	84	42.90%	142
Extended strands	12.99%	43	21.75%	72	12.99%	43
Beta turns	8.46%	28	0.00%	0	10.88%	36
Random coils	36.56%	121	52.87%	175	33.23%	110

Fig.10: Representative examples of Zinc lead compounds consistent with binding mode.

MD simulation of this VEGFR-2 was carried out to assess its stability and to optimize the interactions between the protein and ligand. The RMSD plot showed a general trend for a stable MD trajectory (Fig.9). An initial rise in RMSD was observed for the first 1ns, indicating equilibration of the system. After this equilibration period, the RMSD of the protein-ligand complex over around 6.0Å for the rest of the simulation period, indicating fluctuations in the structure of the protein. MD simulation suggesting that the VEGFR-2 structure is fairly stable.
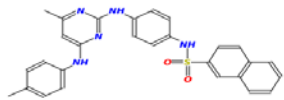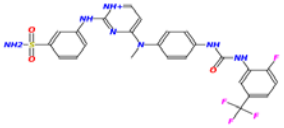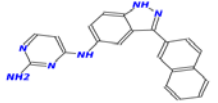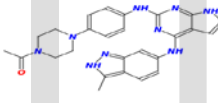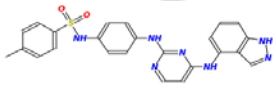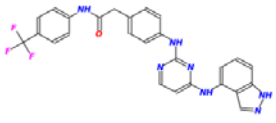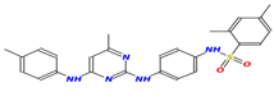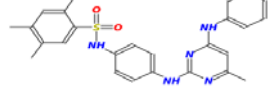
3.5 Sreening ligands
Structure based virtual screening is a proficient approach in discovering inhibitors with novel chemical scaffolds. Two-dimensional structure of Pazopanib was used as query to search for similar compounds in the Zinc database. Then, approximately 35000 compounds were screened and the all compounds were saved for further molecular docking studies.

3.6 Docking studies
Processing of the VEGFR-2 included energy minimized and molecular dynamics simulations. The refinement of structure of protein was used for the dock. AutoDock was used for the docking studies. The docked conformation corresponding to the lowest binding energy was selected as the most probable binding conformation. The total screened 35000 compounds were docked into the active site of VEGFR-2. The docking energies of all the compounds were represented in kcal/mol. The best ten zinc compounds showed best binding energies and significant affinities with target protein of VEGFR-2 the values are represented in Table3. Which all the ligands were embedded within the active site of target protein were observed forming hydrogen bonds with same position as Pazopanib established active site of target protein (Fig.7). The best docked compounds such as Zinc17042891, Zinc14945139, Zinc45339421, Zinc59048015, Zinc45319275, Zinc45228864, Zinc17042880, Zinc17010211, Zinc17026002, Zinc49917676 were found to be shown highest binding energies viz., -11.6, -10.2, -9.9, -8.7, -8.2, -7.6, -7.2, -7.1, -6.4, -6.2kcal/mol respectively (Table3). The zinc lead compounds and their interactions with active site of residues are represented in graphically (Fig.10).

Hydrogen bonds play a role in stabilizing the protein-ligand complex [38]. The screened compounds exhibit several hydrogen bonding moieties. The best binding affinity compounds were obtained from the Zinc database through the structure based virtual screening and molecular docking studies. The screened compounds were docked with active site of VEGFR-2 protein. The compound Zinc14945139 was bound with the affinity -11.0 kcal/mol by the formation of five hydrogen bonds with Asp225, Arg146, Arg146, Asp225 and Asp223 respectively within the active site of target protein. Table3 showed binding energies, protein ligand interactions,

bond angle and bond lengths.

Table3: Binding affinity, bond lengths, and bond angles of the best ten compounds from ZINC database with VEGFR-2

Zinc ID's	Compound structure (2D)	Binding affinity (kcal/mol)	Interactions (Protein-----Ligand)	Bond Angle (degree)	Bond-length(Å)
Zinc17042891		-11.6	1.Gln 15 CO-----$H_{38}N_4$ 2.Glu 13 CO-----N_3H_{41} 3.Glu 13 CO------N_1H_{37} 4.Glu-13 CO ......$H_{37}N_1$ 5.Arg 247 CN......$O_{34}S_{36}$	107.21 92.01 66.26 109.08 123.42	2.06 3.21 3.22 2.34 2.84
Zinc14945139		-10.2	1.Asp225 CO -----N_7H_{45} 2.Arg146 CN ------$O_{34}S_{40}$ 3.Arg146 CN ------$O_{34}S_{40}$ 4.Asp225 CO----- $H_{45}N_7$ 5.Asp223 CO------N_5H_{43}	96.68 90.76 102.91 100.00	3.16 3.02 3.01 3.02
Zinc45339421		-9.9	1.Cys 136 CO-----N_2 H_{28} 2.Lys 137 CO-----N_1H_{33} 3.Leu 57 CO-----N_3 H_{29}	132.76 155.29 145.94	3.05 3.08 2.94
Zinc59048015		-8.7	1.Asp 223 CO-----$O_{36}C_{25}$ 2.Asp 223 CO-----$O_{38}H_{43}$ 3.Glu 134 CO-----N_8H_{40}	68.15 105.98 50.08	3.55 2.97 2.97
Zinc45319275		-8.2	1.Arg 247 CN-----$O_{33}S_{34}$ 2.Tyr 249 CO-----N_4H_{37} 3.Arg 218 CO-----$H_{41}N_7$ 4.Arg218 CO------ N_6H_{39} 5.Gly 215 CO.......$H_{39}N_6$	114.62 102.67 53.58 45.24 123.90	2.87 3.29 3.17 3.05 2.13
Zinc45228864		-7.6	1.Arg 218 CO-----N_7H_{44} 2.Arg 218 CO-----N_6H_6 3.Gly 215 CO-----$H_{41}N_6$ 4.Arg247 CN.......$O_{34}C_{19}$ 5.Glu 13 CO....... N_2H_{43}	115.18 55.53 138.40 98.86 100.61	2.33 2.98 2.15 3.17 3.04
Zinc17042880		-7.2	1.Glu-13 CO-----N_2H_{39} 2.Glu-13 CO-----N_3H_{35} 3.Gly 15 CO-----$H_{37}N_5$ 4.Arg-247 SO--$N_{1992}C_{1993}$	99.66 63.08 107.69 136.26	3.04 2.33 2.13 2.93
Zinc17010211		-7.1	1.Arg247 CO ------$O_{32}S_{34}$ 2.Arg247 CN ------$O_{32}S_{34}$ 3.Arg247 CN ------$O_{32}S_{34}$ 4.Glu 13 CO------ N_2H_{38} 5.Glu13 CO------N_1H_{35}	70.40 16.07 106.18 63.55 24.09	3.92 2.91 3.26 3.03 2.96
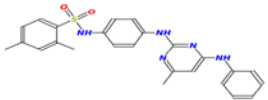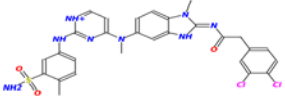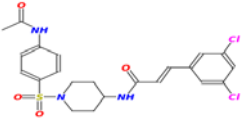
Zinc17026002		-6.4	1.Glu-13 CO -----N_1H_{34} 2.Glu-13 CO ------N_2H37 3.Tyr249 CO------ N_5H_{36} 4.Arg247CN-------$O_{31}S_{33}$	35.11 40.27 57.69 116.34	2.90 3.04 3.20 2.80
Zinc49917676		-6.2	1.LeU 57 CO-----$H_{44}N_3$ 2.LeU 57 CO-----N_3H_{44} 3.Cys 136 CO-----N_8H_{47} 4.Asp 219 CN-----$O_{38}H_{45}$ 5.Asp 219 CO-----$O_{38}H_{45}$	52.14 24.71 31.93 114.50 16.41	3.43 1.83 2.17 3.93 3.38
Pazopanib (Query)		-4.7	1.Lys-137 CO------$H_{34}N_3$	161.9	2.03

Table4: Molecular physical-chemical properties and Lipinski properties of lead molecules of lead compounds with OSIRIS and Molinspiration

Zinc id	M	T	I	R	cLogp	S	MW	Drug likeness	Drug score	H acceptors	H donors	Rotatable bonds
14945139	-	-	-	-	4.35	-3.06	475	-3.63	0.05	10	6	8
17010211	-	-	-	-	4.75	-4.51	305.0	-4.98	0.07	7	3	7
17026002	-	-	-	-	5.78	-6.26	431.0	-9.22	0.04	7	3	7
17042880	-	-	-	-	6.73	-7.3	473.0	-507	0.03	7	3	7
17042891	-	-	-	-	6.66	8.96	479.0	-544	0.03	7	3	7
45228864	-	-	-	-	5.3	-6.43	453.0	-0.62	0.23	8	4	8
45319275	-	-	-	-	4.7	-5.97	457.0	-8.87	0.05	9	5	6
45339421	-	-	-	-	4.62	-6.52	352.0	4.12	0.18	6	4	3
49917676	-	-	+	-	4.89	-9.58	562.0	-0.4	0.04	11	5	7
59048015	-	-	-	-	4.68	-6.25	467.0	2.58	0.09	10	4	5

M: Mutagenisity, **T:** Tumorigenicity, **I:** Irritant, **R:** Reproductive effect, **S:** Solubility.

The MD simulations results revealed that the VEGFR-2-Zinc14945139 (lead1) docking complex maintained high conformational stability (Fig.9) as well as consistent structural flexibility. MD simulations showed novel insight into the natural dynamics of VEGFR-2- Zinc14945139 docking complex by the presence of Water Bridge and additional hydrogen bonds on different time scales. The predicted pharmalogical properties of Zinc14945139 (lead1) was well within the range of a drug molecule with good ADME profile (Tables4) (Lipinski and Hopkins, 2004), hence could be considered for designing inhibitor against VEGFR-2 which in turn would be useful for developing new therapeutic insights on angiogenesis.

4 CONCLUSION

In our work, we have constructed a 3D model of VEGFR-2 using the Modeller9v11. After MD simulations, this refined model structure is obtained. The final refined model was assessed further by SAVES server and the results show that this model is reliable. The stable structure is further used for docking of Screened compounds. Through the docking studies, the model structures of the ligand-protein complex were obtained. The docking results indicate that active site amino-acid residues in VEGFR-2 play an important role in maintaining a functional conformation. The interactions of protein and lig-

ands proposed in this study are useful for understanding the potential mechanisms of VEGFR-2 and the ligands. In particular, with the aid of H2O some hydrogen bonds are formed in the docked complex. As is well known, hydrogen bonds play an important role for the structure and function of biological molecules. On the other hand, the results reported here lead to the proposal of Glu13, Arg247 and Asp225 as key residues because they have strong H-bond contacts with the ligands. These residues are suggested that as candidates for further experimental studies of structure-function relationship. Our investigation revealed that the top ten compounds have exhibited significant binding energies when compare to query (Pazopanib). Zinc14945139 (lead1) showed the best binding energy and pharmalogical profiles among selected leads. The VEGFR-

2 – lead1 docking complex MD simulations revealed that the molecular system was highly stable and its interactions were also highly stable. Therefore, Zinc14945139 is a proposed as best potential inhibitor to designing anti angiogenesis drug.

ACKNOWLEDGMENT

REFERENCES

[1] J.M.Woods, M.Leone, K.Klosowska, P.C.Lamar, T.J.Shaknovsky, W.C. Prozialeck, "Direct antiangiogenic actions of cadmium on human vascular endothelial cells", Toxicol In Vitro, vol. 22, pp. 643–651, 2008.

[2] J.Folkman, "Role of angiogenesis in tumor growth and metastasis", Semin Oncol, vol. 29, pp. 15–18, 2002.

[3] M.V.Blagosklonny, "Antiangiogenic therapy and tumor progression", Cancer Cell, vol. 5, pp. 13–17, 2004.

[4] W.C.Prozialeck, J.R.Edwards, and J.M.Woods, "The vascular endothelium as a target of cadmium toxicity", Life Sci, vol. 79, pp. 1493–1506, 2006.

[5] S.Majumder, A.Muley, G.K.Kolluru, S.Saurabh, K.P.Tamilarasan, S.Chandrasekhar, H.B.Reddy, S.Purohit, and S.Chatterjee, "Cadmium reduces nitric oxide production by impairing phosphorylation of endothelial nitric oxide synthase", Biochem Cell Biol, vol. 86, pp. 1–10, 2008.

[6] M.Helmestam, A.Stavreus-Evers, and M.Olovsson, "Cadmium chloride alters mRNA levels of angiogenesis related genes in primary human endometrial endothelial cells grown in vitro", Reprod Toxicol, vol. 30, pp. 370–376, 2010.

[7] L.Seetharam, N.Gotoh, Y.Maru, G.Neufeld, S.Yamaguchi et al., "A unique signal transduction from FLT tyrosine kinase, a receptor for vascular endothelial growth factor VEGF", Oncogene, vol. 10, pp. 135–147, 1995.

[8] T.V.Petrova, T.Makinen, K.Alitalo, "Signaling via vascular endothelial growth factor receptors", Exp Cell Res, vol. 253, pp. 117–130, 1999.

[9] S.Rousseau, F.Houle, H.Kotanides, L.Witte, J.Waltenberger et al., "Vascular endothelial growth factor (VEGF)-driven actin-based motility is mediated by VEGFR-2 and requires concerted activation of stress-activated protein kinase-2 (SAPK2/p38) and geldanamycin-sensitive phosphorylation of focal adhesion kinase", J Biol Chem, vol. 275, pp. 10661–10672, 2000.

[10] A.K.Olsson, A.Dimberg, J.Kreuger, L.Claesson-Welsh, "VEGF receptor signaling - in control of vascular function", Nat Rev Mol Cell Biol, vol. 7, pp. 359–371, 2006.

[11] M.Shibuya, L.Claesson-Welsh, "Signal transduction by VEGF receptors in regulation of angiogenesis and lymph angiogenesis", Exp Cell Res, vol. 312, pp. 549–560, 2006.

[12] J.H.Baek, J.E.Jang, C.M.Kang, H.Y.Chung, N.D.Kim et al., "Hypoxia induced VEGF enhances tumor survivability via suppression of serum deprivation-induced apoptosis", Oncogene, vol. 19, pp. 4621–4631, 2000.

[13] N.Ferrara, "Vascular endothelial growth factor as a target for anticancer therapy", Oncologist, vol. 9, pp. 2–10, 2004.

[14] R.S.Kerbel, B.A.Kamen, "The anti-angiogenic basis of metronomic chemotherapy", Nat Rev Cancer, vol. 4, pp. 423–436, 2004.

[15] M.E.M.Noble, J. A.Endicott, and L.N.Johnson, "Protein kinase inhibitors: insights into drug design from structure", Science, vol. 303, pp. 1800–1805, 2004.

[16] K.Spiekermann, F.Faber, R.Voswinckel, W.Hiddemann, "The protein tyrosine kinase inhibitor SU5614 inhibits VEGF-induced endothelial cell sprouting and induces growth arrest and apoptosis by inhibition of c-kit in AML cells", Exp Hematol, vol. 30, pp.767–773, 2002.

[17] S.R.Wedge, D.J.Ogilvie, M.Dukes, J.Kendrew, R.Chester et al., "ZD6474 inhibits vascular endothelial growth factor signaling, angiogenesis and tumor growth following oral administration", Cancer Res, vol. 62, pp. 4645–4655, 2002.

[18] B.Sloan, N.Scheinfeld, S.A.Pazopanib, "VEGF receptor tyrosine kinase inhibitor for cancer therapy", Curr Opin Investig Drugs, vol. 9, pp. 1324-35, 2008.

[19] A.Sali, T.L.Blundell, "Comparative protein modelling by satisfaction of spatial restraints", J Mol Biol, vol. 234, pp. 779–815, 1993.

[20] M.Camila, A.Francisco, H.Jans, M.Alzate, A.Vergara-Jaque, T.Kniess, J.Caballero, "Study of differences in the VEGFR2 inhibitory activities between semaxanib and SU5205 using 3D-QSAR, docking, and molecular dynamics simulations", J Mol Graph Model, vol. 32, pp. 39–48, 2012.

[21] J.D.Thompson, D.G.Higgins, T.J.Gibson, "CLUSTAL W: Improving the sensitivity of progressive multiple sequence alignment through sequence weighting, position-specific gap penalties and weight matrix choice", Nucl Aci Res, vol. 22, pp. 4673–4680, 1994.

[22] M.A.Marti-Renom, A.C.Stuart, A.Fiser, R.Sanchez, F.Melo, A.Sali, "Comparative protein structure modeling of genes and genomes", Annu Rev Biophys Biomol Struct, vol. 29, pp. 291–325, 2000.

[23] M.Y.Shen, A.Sali, "Statistical potential for assessment and prediction of protein structures", Protein Sci, vol. 15, pp. 2507–2524, 2006.

[24] R.A.Laskoswki, M.W.MacArthur, D.S.Moss, J.M.Thornton, "PROCHECK: A program to check the stereo chemical quality of protein structures", J. Appl. Cryst, vol. 26, pp. 283-291, 1993.

[25] M.D.Eisenberg, R.Luthy, J.U.Bowie, "VERIFY3D: assessment of protein models with three-dimensional profiles", Methods Enzymol, vol. 277, pp. 396-404, 1997.

[26] C.Colovos, T.O.Yeates, "Verification of protein structures: Patterns of nonbonded atomic interactions", Protein Sci, vol. 2, pp. 1511-9, 1993.

[27] G.Vriend, "WHAT IF: a molecular modeling and drug design program", J Mol Graph, vol. 8, pp. 52–56, 1990.

[28] R.W.W.Hooft, C.Sander, and G.Vriend, "Verification of protein structures: Side-chain planarity", J Appl Crystallogr, vol. 29, pp. 714–716, 1996.

[29] W.Humphrey, A.Dalke, K.Schulten, "VMD: visual molecular dynamics", J Mol Graph, vol. 14, pp. 33-8, 27-8, 1996.

[30] A.D.MacKerell et al., "All-atom empirical potential for molecular modeling and dynamics studies of proteins", J Phys Chem, vol. 102, pp. 3586-3616, 1998.

[31] J.Dundas, Z.Ouyang, J.Tseng, A.Binkowski, Y.Turpaz, J.Liang, "CASTp: computed atlas of surface topography of proteins with structural and topo-

graphical mapping of functionally annotated residues", Nucleic Acids Res, vol. 34, pp. W116–W118, 2006.

[32] J.Dundas, Z.Ouyang, J.Tseng, A.Binkowski, Y.Turpaz, J.Liang, "CASTp: computed atlas of surface topography of proteins with structural and topographical mapping of functionally annotated residues", Nucleic Acids Res, vol. 34, pp. W116–W118, 2006.

[33] C.A.Lipinski, F.Lombardo, B.W.Dominy, P.J.Feeny, "Experimental and computational approaches to estimate solubility and permeability in drug discovery and development settings", Adv Drug Delivery Rev, vol. 23, pp. 3–25, 1997.

[34] D.F.Veber, S.R.Johnson, H.Y.Cheng, B.R.Smith, K.W.Ward, K.D.Kopple, "Molecular properties that influence the oral bioavailability of drug candidates", J Med Chem, vol. 6, pp. 2615-23, 2002.

[35] L.K.Wolf, "PyRx", C&EN, vol. 87, pp. 31, 2009.

[36] O.Trott, A.J.Olson, "AutoDock Vina: improving the speed and accuracy of docking with a new scoring function, efficient optimization, and multithreading", J Comput Chem, vol. 31, pp. 455–461, 2010.

[37] F.Gao, N.Bren, T.P.Burghardt, S.Hansen, R.H.Henchman, P.Taylor, J.A.McCammon, S.M.Sine, "Agonist-mediated conformational changes in acetylcholine-binding protein revealed by simulation and intrinsic tryptophan fluorescence", J Biol Chem, vol. 280, pp. 8443–8451, 2005.

[38] J.J.Irwin, B.K.Shoichet, "ZINC-a free database of commercially available compounds for virtual screening", J Chem Inf Model, vol. 45, pp. 177–182, 2005.

[39] J.J.Irwin, B.K.Shoichet, "ZINC-a free database of commercially available compounds for virtual screening", J Chem Inf Model, vol. 45, pp. 177–182, 2005.

[40] N.Ferrara, R.S.Kerbel, "Angiogenesis as a therapeutic target", Nature, vol. 438, pp. 967–974, 2005.